

RESEARCH ARTICLE

Multiple model fault diagnosis and fault tolerant control for the launch vehicle's attitude control system

X. Chang-lin¹, Y. Shu-ming¹, C. Yu-qiang and S. Li-jun

College of Aerospace Science and Engineering, National University of Defense Technology, Changsha, Hunan 410073, China

Corresponding author: Y. Shu-ming; Email: yangshuming07@nudt.edu.cn

Received: 12 July 2023; **Revised:** 17 January 2024; **Accepted:** 25 January 2024

Keywords: launch vehicle; fault diagnostics; fault tolerant control; kalman filters; sensor fault; actuator fault

Abstract

For the launch vehicle attitude control problem, traditional methods can seldom accurately identify the fault types, making the control method lack of pertinence, which largely affects the effect of attitude control. This paper proposes an active fault tolerant control strategy, which mainly includes fault diagnosis and fault tolerant control. In the fault diagnosis part, a small deviation attitude dynamics model of the launch vehicle is established. Kalman filters with different structures are designed to detect and isolate faults through residual changes, and the fault quantity of the actuator is further estimated. In the fault tolerant control part, the following control scheme is adopted according to the above diagnostic information: when the sensor fault is detected, the sensor measurement data is reconstructed; when the actuator fault is identified, the control allocation matrix is reconstructed. Simulation results show that the proposed method can effectively diagnose sensor fault and actuator faults, and significantly improve attitude tracking accuracy and control adjustment time.

Nomenclature

FTC	fault tolerant control
ACS	attitude control system
FDD	fault detection and diagnosis
EKF	extended Kalman filter
CAM	control allocation matrix
MMFD	multiple model fault diagnosis
i-ACEKF	the i-th actuator corresponds to the EKF
ACEKF	actuator corresponds to the extended Kalman filter
SCKF	the sensor corresponds to the Kalman filter
j-SCKF	the j-th sensor corresponds to the Kalman filter
WSSR	the weighted sum of squares of residual
BCL	basic control law
CDL	control distribution law
ABSA-1	actuator booster swing angle 1

1.0 Introduction

With the booming space activities in today's world and the increasing demand for international commercial launches, the development of a new generation of launch vehicles is the key to future space development planning [1]. The attitude control system (ACS), as the core system of the launch vehicle, has a complex structure and is prone to failure. According to statistics, ACS failures account for more

than 60% of all system failures [2]. Fault diagnosis and FTC technology can make full use of the fault information through parameter adjustment, control reconfiguration and other measures so that the system can maintain a certain control performance under the fault state to ensure the successful completion of the mission, which has been widely used in the design of aerospace flight control systems.

The existing fault detection and diagnosis (FDD) techniques are mainly classified into three types of methods, model-based, data-based and knowledge-based. Considering the easy availability of ACS mathematical models and the scarcity of flight history data, model-based fault diagnosis methods occupy the majority of the research, particularly, the methods for diagnosing by establishing observers have attracted wide attention [3]. For example, in [4], an actuator fault diagnosis method was studied for the design of corresponding observers for satellite attitude control systems. In [5], the fault-tolerant control of a flight control system under sensor/actuator failure is accomplished using the Kalman filter technique and control reconstruction approach. A sliding film controller is utilised to accomplish high-precision tracking of the attitude with finite-time convergence in [6], which investigates an adaptive finite-time extended state observer to estimate the brake failure of the attitude system. According to [7], a collection of full-order linear parameter-varying unknown input observers is intended to identify, distinguish, and estimate sensor parameters for nonlinear system failure detection.

Fault tolerant control (FTC) techniques are mainly categorised into passive fault tolerant control and active fault tolerant control, which can ensure the stability of the system while effectively compensating for the fault loss. Most of the existing passive FTC techniques are based on Lyapunov functions and use theoretical methods to construct fault tolerant controllers, such as smooth mode control [8], adaptive control [9] and backward control [10]. However, the design and derivation forms of such controllers are too complex, and most of them are only for a single fault mode, which makes it difficult to ensure the stability of control under extreme faults. Due to the limited onboard storage space and computational capability, passive FTC is rarely used in practical engineering.

The main difference between active FTC over passive FTC is that the structure of this sort of controller is not fixed, and the gain or structure may be altered by giving fault information via the FDD module [11]. For example, an unscented Kalman filter based on a multimodel approach integrated with a PD controller for active FTC was built for a precise estimate of the attitude control system [12]. To effectively increase the rocket attitude tracking accuracy, an adaptive fault observer is built in [13], and the sliding model fault-tolerant controller is devised on this premise. In [14], backstepping and adaptive methods are used with fault observation information to develop an active fault-tolerant controller. According to [15], a spacecraft attitude FTC is implemented using an adaptive learning observer based on a backpropagation controller. It can be seen that this type of control method has strong autonomy, diversified design methods, and means, makes full use of analysis redundancy, and can reasonably ensure the stability of the system in the event of known or unknown faults with the advantages of system hardware and software. Additionally, the use of active FTC approaches in aircraft engineering is mostly successful. Examples of this include the Falcon 9 rocket, which used fault diagnostic and online reprogramming techniques to launch an engine with thrust failure during the maiden ISS flight in 2012 and complete the mission. Additionally, the Chinese CZ-5 new-generation launch vehicle successfully achieved attitude stability control after the booster engine was turned off by using the engine control force dynamic distribution technology [1].

In order to better realise the FTC of the system, inspired by the previous studies, this paper proposes a multimodel fault diagnosis (MMFD) and FTC algorithm to accurately track and stabilise the rocket's attitude angle, taking into account a variety of typical failure modes. The following is the paper's structure. The launch vehicle minor deviation attitude dynamics model is established in Chapter 2. In Chapter 3, numerous Kalman filters with different topologies are built to model the features of actuator and sensor failure, respectively. The technique and approach for fault identification and isolation are proposed in Chapter 4. The fault diagnostic information is used in Chapter 5 to perform FTC. Chapter 6 conducts simulation research to validate the efficacy of the multiple-model fault diagnosis and FTC algorithm. Chapter 7 is the conclusion.

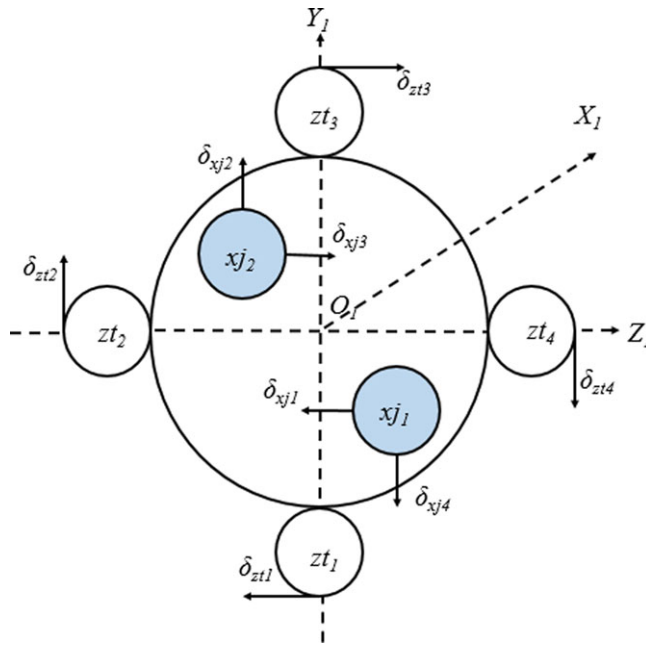


Figure 1. Engine layout of some strap-on launch vehicles from the bottom view [24].

2.0 Research subject analysis

This paper considers a large Chinese launch vehicle the Long March 5B, which is primarily responsible for launching the core modules and experimental modules of the space station, and is currently the heaviest Chinese rocket with near-Earth orbit capability, with a takeoff weight of about 837.5 tons [16]. There are eight swing angles at the tail part of the arrow body, among them, δx_{j1} , δx_{j3} , and δz_{t1} , δz_{t3} control the pitch channel, δx_{j2} , δx_{j4} and δz_{t2} , z_{t4} control the yaw channel. The eight swing angles control the roll channel of the rocket. The engine layout and swing mode are shown in Fig. 1 below.

The rocket channels are decoupled and the small deviation attitude dynamics are modeled as follows.

$$\ddot{\varphi} + b_1^\varphi \Delta \dot{\varphi} + b_2^\varphi \Delta \alpha + b_{3x}^\varphi \Delta \delta_{\varphi xj} = b_{3x}^{\varphi} \Delta \ddot{\delta}_{\varphi xj} + b_{3z}^\varphi \Delta \delta_{\varphi zt} + b_{3z}^{\varphi} \Delta \ddot{\delta}_{\varphi zt} = \bar{M}_{BZ1} - b_2^\varphi (\alpha_{wp} + \alpha_{wq}) \quad (1)$$

$$\ddot{\psi} + b_1^\psi \dot{\psi} + b_2^\psi \psi - b_{3xj1}^\psi \Delta \delta_{xj1} + b_{3xj2}^\psi \Delta \delta_{xj3} - b_{3zt1}^\psi \Delta \delta_{zt1} + b_{3zt3}^\psi \Delta \delta_{zt3} = \bar{M}_{BY1} - b_2^\psi (\beta_{wp} + \beta_{wq}) \quad (2)$$

$$\ddot{\gamma} + d_1 \dot{\gamma} + d_{3x} \delta_{\gamma xj} + d_{3x}^{\gamma} \ddot{\delta}_{\gamma xj} + d_{3z} \delta_{\gamma zt} + d_{3z}^{\gamma} \ddot{\delta}_{\gamma zt} = \bar{M}_{BX1} \quad (3)$$

where $\Delta \varphi$, ψ , γ , $\Delta \theta$, $\Delta \alpha$, σ , β are the deviations of the rocket's attitude angle from each Euler angle during flight, respectively, $\Delta \delta_{\varphi zt}$, $\Delta \delta_{\psi zt}$, $\Delta \delta_{\gamma zt}$ are equivalent swing angle commands for booster engines, $\Delta \delta_{\varphi xj}$, $\Delta \delta_{\psi xj}$, $\Delta \delta_{\gamma xj}$ are the equivalent swing angle command for the core stage engine. The detailed derivation procedure and symbolic meaning are presented in [17].

If we set,

$$x = [\Delta \varphi \ \Delta \dot{\varphi} \ \psi \ \dot{\psi} \ \gamma \ \dot{\gamma}] \quad (4)$$

$$u = [\delta_{xj1} \ \delta_{xj2} \ \delta_{xj3} \ \delta_{xj4} \ \delta_{zt1} \ \delta_{zt2} \ \delta_{zt3} \ \delta_{zt4}] \quad (5)$$

$$M = [0 \ \bar{M}_{BZ1} - b_2^\varphi (\alpha_{wp} + \alpha_{wq}) \ 0 \ \bar{M}_{BY1} - b_2^\psi (\beta_{wp} + \beta_{wq}) \ 0 \ \bar{M}_{BX1}] \quad (6)$$

the system state equation may be written as

$$\begin{cases} \dot{x} = Ax + Bu + M + w \\ y = Cx + v \end{cases} \quad (7)$$

where x , y , and u are state variables, sensor measured values, and control commands, respectively, A , B , C , and M are the state matrix; w , v are system noise and measurement noise, respectively, they are uncorrelated Gaussian white noise, i.e.

$$E[w(k)] = E[v(k)] = 0 \quad (8)$$

$$E[w(k), w^T(j)] = Q(k)\tau_{kj} \quad (9)$$

$$E[v(k), v^T(j)] = R(k)\tau_{kj} \quad (10)$$

where $\tau_{kj} = \begin{cases} 1, & k=j \\ 0, & k \neq j \end{cases}$

The system is sampled at the moment $t(k) = kT$. By discretising Equation (7), we could obtain

$$\begin{cases} x(k+1) = F(k)x(k) + D(k)u(k) + M(k) + w(k) \\ y(k) = Hx(k) + v(k) \end{cases} \quad (11)$$

where $F(k) = AT + I$, $D(k) = BT$, $H(k) = C$.

Assuming the system is completely scalable, the Kalman filtering algorithm flow is as follows [18].

- 1) Prediction equation. The result of the previous step is used as the initial value for this calculation. As shown in Equations (12) and (13).

$$\hat{x}(k|k-1) = F(k-1)\hat{x}(k-1|k-1) + D(k-1)u(k-1) + M(k-1) \quad (12)$$

$$P(k|k-1) = F(k-1)P(k-1|k-1)F(k-1)^T + E(k-1)Q(k-1)E(k-1)^T \quad (13)$$

- 2) The Kalman gain matrix is calculated.

$$K(k) = P(k|k-1)H^T[HP(k|k-1)H^T + R(k)]^{-1} \quad (14)$$

- 3) Updates the equation.

$$P(k|k) = [I - K(k)H]P(k|k-1) \quad (15)$$

$$\hat{x}(k|k) = \hat{x}(k|k-1) + K(k)[y(k) - H\hat{x}(k|k-1)] \quad (16)$$

Where the initial conditions are

$$\hat{x}(0) = x_0, \quad P(0|0) = P_0 \quad (17)$$

The Kalman filter residual for this system is

$$\Delta r(k) = y(k) - H(k)\hat{x}(k|k-1) \quad (18)$$

When a system fault occurs, the residuals change rapidly, and statistical features can be analysed to detect system faults. However, the above generalised Kalman filter can only identify faults and cannot isolate the type of fault or diagnose the size of the problem. For this reason, this paper proposes an MMFD algorithm to realise the FDD of the system and at the same time provide effective information for the FTC of the system.

3.0 The design of the Kalman filter set

The Kalman filter of the corresponding structure is built using the features of actuator and sensor failures. First, the methods for detecting actuator faults and estimating parameter values are presented.

3.1 Actuator malfunction

Typical failures of launch vehicle actuators include engine swing angle jamming, actuator damage, and loose float swing [19]. The real swing angle of the i -th actuator failure can be represented as

$$u'_i = u_i + e_i (\tilde{\delta}_i - u_i) \tag{19}$$

where u'_i is the true swing angle value after the failure of the i -th actuator, e_i is the non-zero matrix ($e_i = 1, e_j = 0, i \neq j$), $\tilde{\delta}_i$ is the magnitude of the failure of the i -th actuator. The system equation of state after the i -th actuator failure is as follows.

$$\begin{cases} x(k+1) = F(k)x(k) + D^{remain}(k)u(k) + D^i(k)\tilde{\delta}_i(k) \\ \quad + M(k) + w(k) \\ y(k) = Hx(k) + v(k) \end{cases} \tag{20}$$

where $D^i(k)$ is the i -th column of the matrix, $D^{remain}(k)$ is the matrix after the i -th column of the matrix is set to zero.

To obtain information about the actuator failure parameters, the state variables of Equation (4) are extended as follows,

$$\bar{x}(k) = \begin{cases} x(k) \\ \tilde{\delta}_i(k) \end{cases} \tag{21}$$

Then the equation of state can be expressed as

$$\begin{cases} \bar{x}(k+1) = G(k) \begin{bmatrix} x(k) \\ \tilde{\delta}_i(k) \end{bmatrix} + L(k)u(k) + \begin{bmatrix} 1 \\ 0 \end{bmatrix} M(k) + w(k) \\ y(k) = [H \ 0] \begin{bmatrix} x(k) \\ \tilde{\delta}_i(k) \end{bmatrix} + v(k) \end{cases} \tag{22}$$

where $G(k) = \begin{bmatrix} F(k) & D^i(k) \\ 0 & 1 \end{bmatrix}$, $L(k) = \begin{bmatrix} D^{remain}(k) \\ 0 \end{bmatrix}$.

From the system in Equation (22), the Kalman filter equation for the i -th actuator fault is obtained [20].

$$\bar{x}_i(k|k-1) = \begin{bmatrix} \hat{x}_i(k|k-1) \\ \hat{\delta}_i(k|k-1) \end{bmatrix} \tag{23}$$

$$\hat{x}_i(k|k-1) = F(k-1)\hat{x}_i(k-1|k-1) + D^{remain}(k-1)u(k-1) + M(k-1) \tag{24}$$

$$P_i(k|k-1) = G(k-1)P_i(k-1|k-1)G(k-1)^T + E(k-1)Q(k-1)E(k-1)^T \tag{25}$$

$$K_i(k) = P_i(k|k-1)H^T [HP_i(k|k-1)H^T + R(k)]^{-1} \tag{26}$$

$$P_i(k|k) = [I - K_i(k)H] P_i(k|k-1) \tag{27}$$

$$\bar{x}_i(k|k) = \bar{x}_i(k|k-1) + K_i(k) [y(k) - H\bar{x}_i(k|k-1)] \tag{28}$$

At time $k + 1$, the i -th actuator corresponds to the EKF (i-ACEKF), which can be represented as

$$\begin{aligned} \Delta r_i(k + 1) = y(k + 1) - H\hat{x}_i(k + 1|k) = y(k + 1) - [F(k)\hat{x}_i(k|k) + D^{remain}(k)u(k) \\ + M(k)] = HF(k) [x_i(k) - \hat{x}_i(k|k)] + D^i(k)\tilde{\delta}_i(k) + v(k + 1) \end{aligned} \tag{29}$$

This research focuses solely on the failure of a single actuator. When the i -th actuator does not fail, the corresponding residual value follows a multivariate distribution with a zero mean; when the i -th actuator fails, the corresponding residual value $\Delta r_i(k)$ abruptly changes, allowing the associated failure to be discovered and isolated.

3.2 Sensor malfunction

The platform and rate gyroscope are used to measure the attitude angle and angular rate of the carrier rocket, respectively [21]. According to the different sensor installation positions, the measurement signal can be expressed as

$$\Delta\varphi_{zt} = \Delta\varphi - \sum_p W_p'(x_T) q_p \tag{30}$$

$$\Delta\varphi_s = \Delta\dot{\varphi} - \sum_p W_p'(x_s) \dot{q}_p \tag{31}$$

where $w_p'(x_T)$ is the slope of the p -th oscillation at the attitude angle measurement device installation, $w_p'(x_s)$ is the slope of the p -th oscillation at the velocity gyro mounting.

The main manifestations of the launch vehicle sensor failure are jamming, bias, increased drift, and increased noise [19]. Since the structure of the sensor corresponds to the Kalman filter (SCKF) is relatively simple, and the coupling between filter equations is weak. When only the sensor fails, the system (11) can be rewritten as

$$\begin{cases} x(k + 1) = F(k)x(k) + D(k)u(k) + M(k) + w(k) \\ \begin{bmatrix} y_j(k) \\ y_{remain}(k) \end{bmatrix} = \begin{bmatrix} H_j \\ H_{remain} \end{bmatrix} x(k) + v(k) + \begin{bmatrix} f_j(k) \\ f_{remain}(k) \end{bmatrix} \end{cases} \tag{32}$$

where $y_j(k), f_j(k)$ are the j -th row of the system output vector and the sensor fault vector, respectively, $y_{remain}(k), f_{remain}(k)$ are the remaining rows of the system output vector and sensor fault vector, respectively. H_j is the j -th row of the H matrix in Equation (11), H_{remain} is the remaining row of the H-matrix in the system.

According to the system in Equation (32), the Kalman filter equation when the j -th sensor fails can be obtained.

$$\hat{x}_j(k|k - 1) = F(k - 1)\hat{x}_j(k - 1|k - 1) + D(k - 1)u(k - 1) + M(k - 1) \tag{33}$$

$$P_j(k|k - 1) = F(k - 1)P_j(k - 1|k - 1)F(k - 1)^T + E(k - 1)Q(k - 1)E(k - 1)^T \tag{34}$$

$$K_j(k) = P_j(k|k - 1)H_j^T [H_jP_j(k|k - 1)H_j^T + R(k)]^{-1} \tag{35}$$

$$P_j(k|k) = [I - K_j(k)H_j] P_j(k|k - 1) \tag{36}$$

$$\hat{x}_j(k|k) = \hat{x}_j(k|k - 1) + K_j(k) [y_j(k) - H_j\hat{x}_j(k|k - 1)] \tag{37}$$

The j -th sensor corresponds to the Kalman filter (j-SCKF) at moment $k + 1$ can be expressed as

$$\begin{aligned} \Delta r_j(k + 1) = y_j(k + 1) - H_j\hat{x}_j(k + 1|k) = y(k + 1) - [F(k)\hat{x}_j(k|k) + D(k)u(k) + M(k)] \\ = H_jF(k) [x(k) - \hat{x}_j(k|k)] + f_j(k + 1) + v(k + 1) + w(k) \end{aligned} \tag{38}$$

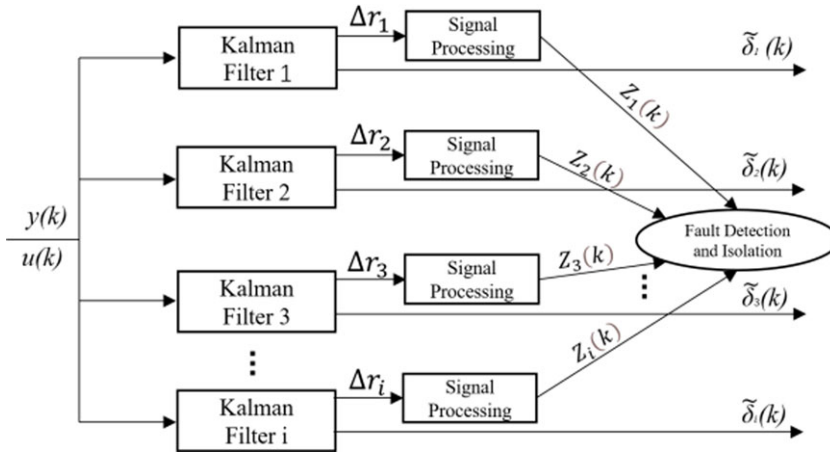


Figure 2. Flowchart of launch vehicle actuator based on MMFD algorithm.

From Equation (38), if the state estimate is unbiased at the initial moment when the j -th sensor is without failure i.e., $f_i = 0$, the state estimated by the j -SCKF is unbiased for system (32) and the residuals conform to the multivariate distribution with zero mean; when a fault occurs in the j -th sensor, i.e., $f_i \neq 0$, the residual has changed, so that the failure can be detected and isolated and has no effect on the residuals of the remaining SCKF.

4.0 The multimodel fault diagnosis algorithm isolation strategy

4.1 The flow of the multimodel fault diagnosis algorithm

The MMFD algorithm developed in this research is applicable to actuator or sensor failures in any state of the carrier rocket. In order to reduce the influence of noise on the diagnosis results, the sum of the weighted squares algorithm is used to process the residual signal, and the formula is as follows.

$$Z_r(k) = \frac{1}{N + 1} \sum_{\tau=k-N}^k \Delta_r^T(\tau) \Delta_r(\tau) \tag{39}$$

where N is the length of the data window. When N is increased, the robustness of the system detection increases, and the likelihood of false alarms decreases, but the system’s computation amount increases.

The idea of a classical special observer is applied to the failure of the launch vehicle actuator, and the principle of fault detection and isolation based on the MMFD algorithm is shown in Fig. 2, where Δr_i is the residual, which is the difference between the predicted output value of the Kalman filter and the measured value.

The fault detection and isolation process based on the MMFD algorithm is also obtained for the launch vehicle sensor, as illustrated in Fig. 3. And the signal processing modules in Figs. 2 and 3 correspond to the noise reduction processing shown in formula (39).

In order to improve detection accuracy and reduce the rate of false alarm and false alarms, a twofold threshold is used for fault detection. After determining the detection threshold DT and absolute threshold, the dual threshold detection method is as follows.

- 1) When the weighted sum of squares of residuals (WSSR) $Z_r(k)$ exceeds the detection threshold for three consecutive moments, it is regarded to have a failure, i.e., $Z_r(k) > DT$, where $k = t, t + 1, t + 2$.

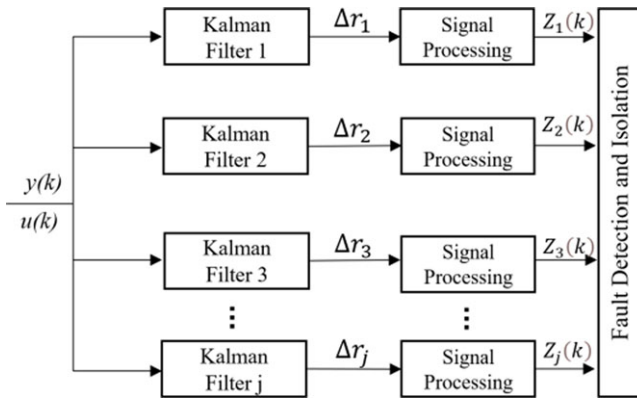


Figure 3. Flowchart of launch vehicle sensor based on MMFD algorithm.

- 2) When the WSSR $Z_{\tau}(k)$ exceeds the absolute threshold at a certain time, it is considered to have a failure, i.e., $Z_{\tau}(k) > DT_{Max}$.

4.2 Isolation strategy based on multimodel fault diagnosis algorithm

The above methods can only detect and isolate a single fault. In order for the diagnostic system to be able to detect and isolate both actuator and sensor faults, a corresponding isolation strategy needs to be derived.

Since the weak coupling of the SCKF set, the first localisation of faults is performed using this filter set. We can deduce from Equation (38) that several sets of SCKF residuals exceed the threshold when an actuator fails. Considering the extremely low probability of multiple sensors failing at the same time, the multifault isolation technique based on the MMFD algorithm is as follows.

- 1) When only one set of WSSR of SCKF exceeds the threshold, it indicates that the sensor is defective and can be recognised directly.
- 2) When multiple sets of WSSR of SCKF exceed the threshold, it indicates that the actuator is faulty. Then, the actuator corresponding to the EKF (ACEKF) group is utilised to achieve further isolation and localisation. The multifault isolation strategy of the launch vehicle is shown in Fig. 4.

On the basis of the above method, the fault detection and isolation of actuators and sensors were accomplished. Further, richer actuator fault information was obtained by utilising EKF, laying the foundation for FTC of the launch vehicle.

5.0 Fault tolerant control under launch vehicle failure

The ACS is broken into two parts: the basic control law (BCL) and the control distribution law (CDL). Among them, the BCL generally includes the PD control and correction network, whose primary duty is to calculate the rocket attitude angle information measured on the arrow during flight through the basic control law to obtain the virtual control commands for the three channels of rocket pitch, yaw and roll ($\delta_{\varphi}^s, \delta_{\psi}^s, \delta_{\gamma}^s$); The commands of the BCL are then assigned to the core and boost channels according to a predetermined distribution ratio to obtain the respective equivalent swing angle commands ($\delta_{\varphi xj}^s, \delta_{\psi xj}^s, \delta_{\gamma xj}^s$ and $\delta_{\varphi zt}^s, \delta_{\psi zt}^s, \delta_{\gamma zt}^s$). The CDL's purpose is to deliver comparable swing angle orders to the servo mechanisms on the core stage and boost motors, causing each swing motor to swing to create control torque and, ultimately, adjust the rocket's flying attitude. Figure 5 illustrates the specific flow.

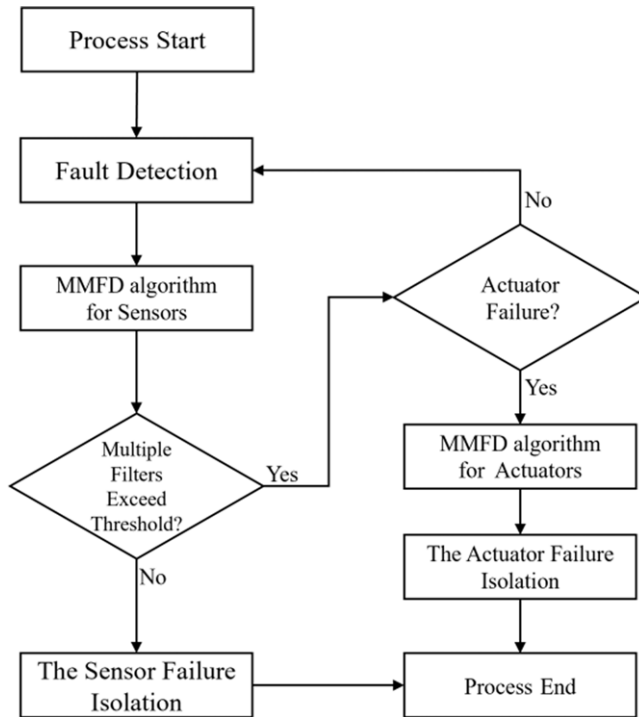


Figure 4. Multi-fault detection and isolation strategy of launch vehicles.

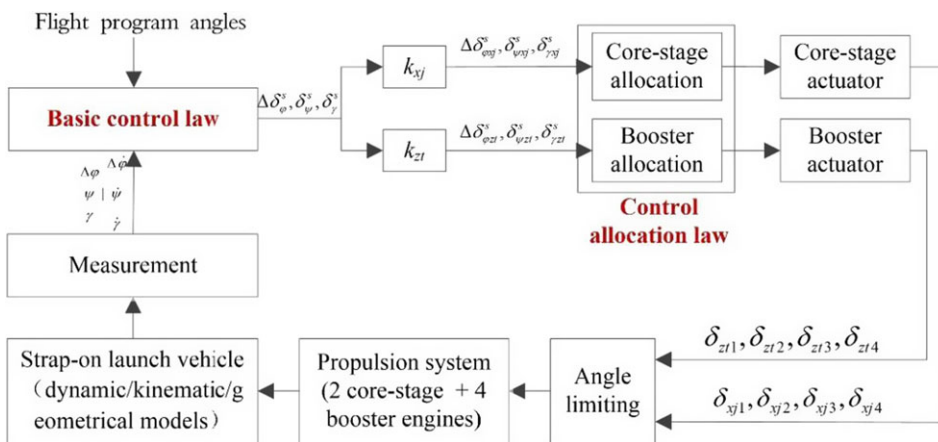


Figure 5. Structure of launch vehicle attitude control system [24].

5.1 Fault tolerant control under actuator failure

The CDL redistributes the engine swing angle so that the redistributed control torque is equal to the desired generated control torque to achieve FTC under the rocket fault, with the following mathematical expression (the detailed derivation process is shown in Appendix A).

$$\begin{bmatrix} b_{3x}^\varphi \Delta \delta_{\varphi xj}^s + b_{3z}^\varphi \Delta \delta_{\varphi zt}^s \\ b_{3x}^\psi \delta_{\psi xj}^s + b_{3z}^\psi \delta_{\psi zt}^s \\ d_{3x}^s \delta_{\gamma xj}^s + d_{3z}^s \delta_{\gamma zt}^s \end{bmatrix} = \begin{bmatrix} 0 & -b_{3xj2}^\varphi & 0 & b_{3xj1}^\varphi & 0 & -b_{3zt2}^\varphi & 0 & b_{3zt4}^\varphi \\ -b_{3xj1}^\varphi & 0 & b_{3xj2}^\varphi & 0 & -b_{3zt1}^\varphi & 0 & b_{3zt3}^\varphi & 0 \\ d_{3x1} & d_{3x2} & d_{3x3} & d_{3x4} & d_{3z1} & d_{3z2} & d_{3z3} & d_{3z4} \end{bmatrix} \times \begin{bmatrix} \delta_x \\ \delta_z \end{bmatrix} \quad (40)$$

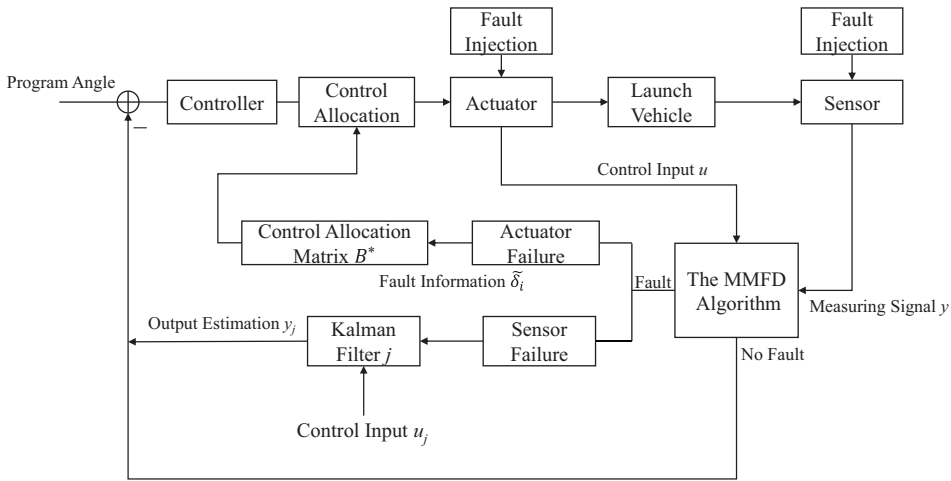


Figure 6. Flow chart of launch vehicle active FTC.

where $b_{3x}^\phi, b_{3z}^\phi, b_{3xj1}^\phi, b_{3xj2}^\phi, b_{3zj2}^\phi, b_{3zj4}^\phi, b_{3x}^\psi, b_{3z}^\psi, b_{3xj1}^\psi, b_{3xj2}^\psi, b_{3zj3}^\psi, b_{3zj3}^\psi, d_{3x}, d_{3z}, d_{3x1-4}, d_{3z1-4}$ are the coefficients of rigid body motion equations, and the detailed meanings can be seen in reference [17]. $\Delta\delta_{\phi xj}^s, \Delta\delta_{\phi zj}^s, \delta_{\psi xj}^s, \delta_{\psi zj}^s, \delta_{\gamma xj}^s, \delta_{\gamma zj}^s$ are the equivalent swing angle instruction of core stage and boost, $\delta_x = [\delta_{x1} \delta_{x2} \delta_{x3} \delta_{x4}]^T$, $\delta_z = [\delta_{z1} \delta_{z2} \delta_{z3} \delta_{z4}]^T$ are the swing angle of the core stage and the boost engine, as shown in Fig. 5.

It can be expressed as

$$M = Bu \tag{41}$$

where M is the desired torque, B is the CAM.

If an actuator fails, the MMFD algorithm isolates the failure features of the i -th actuator, and this failure information is integrated into the ACS.

At moment k , the actual swing angle after the failure of the i -th actuator is shown in Equation (19), then the CAM at this point can be expressed as

$$B^* = [B_{remain} \ B_i] \begin{bmatrix} u_{remain} \\ \delta_i \end{bmatrix} \tag{42}$$

where B_i is the column vector of the CAM corresponding to the i -th actuator, B_{remain}, u_{remain} are the remaining columns of the CAM and the remaining rows of the actuator, respectively.

When the i -th actuator malfunctions, we may inverse solve for the magnitude of the remaining swing angle after redistribution by the CAM, i.e.

$$u' = (B^*)^{-1}M \tag{43}$$

Based on the above method, FTC under actuator failure is achieved, as shown in Fig. 6.

5.2 Fault tolerant control under sensor failure

After using the MMFD algorithm for fault detection of the launch vehicle, if only the faulty sensors are separated, it will lead to a reduction of the monitored measurement parameters, which will not accurately reflect the flight attitude of the rocket and affect the normal operation of the controller.

Considering that the input variables of the j th filter do not contain faulty sensor data at the moment of fault, an accurate estimation of output and state variables can be realised. According to the system in Equation (11), the fault data of the j th sensor is replaced with the corresponding estimated data as shown in Fig. 6.

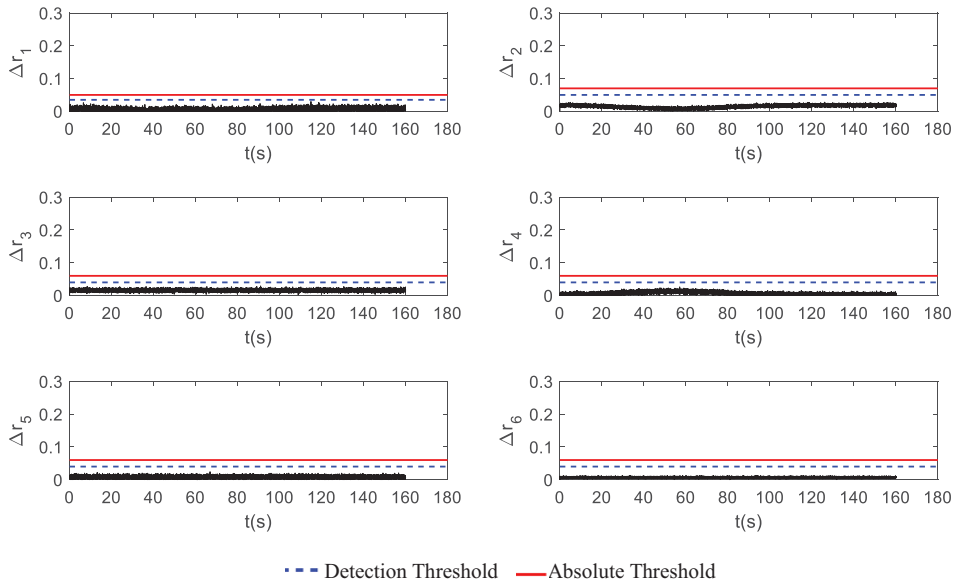


Figure 7. The SCKF group diagram of the faultless state.

Fault injection is used to simulate defects during rocket flight, as shown in Fig. 6. When no fault is present, the measured signal y is directly output; when a fault is present, the MMFD method is used to detect and isolate faults of various fault types and to calculate the category and magnitude of the fault. Finally, the necessary reconfiguration steps are performed to mitigate the effects of the problem and restore system performance.

6.0 Numerical validations

To validate the efficiency of the suggested strategy, simulation analysis is performed for several launch vehicle failure scenarios. This study proposes eight Kalman filters for the FDD of actuators, as well as six Kalman filters for the FDD of sensors.

6.1 Faultless state

When the launch vehicle operates correctly, none of the residuals of SCKF and ACEKF weighted square values surpass the threshold value, as seen in Figs. 7 and 8.

It can be seen that when the system does not fail, there is a certain correspondence between the core stage engine swing angle and the boost engine swing angle, so the simulation curve of $\Delta r_5 \sim \Delta r_8$ is also similar to $\Delta r_1 \sim \Delta r_4$, which is close to the zero-mean multivariate distribution. Due to the influence of wind interference, noise, and other factors, some of the residual values have slight fluctuations, but none of them exceed the set threshold.

The estimated value of the pendulum angle of the actuator corresponding to the EKF in the absence of faults is given in Fig. 9, and the actual value in the figure is the normal state value of the system. Due to no change in the rocket control torque, the actuator’s pendulum angle value is close to zero.

Combining Figs. 7–9, it is clear that the ACEKF may estimate the angle of each pendulum angle of the actuator. Under fault-free conditions, the MMFD algorithm can perform health detection of the state of the launch vehicle servo mechanism or sensor.

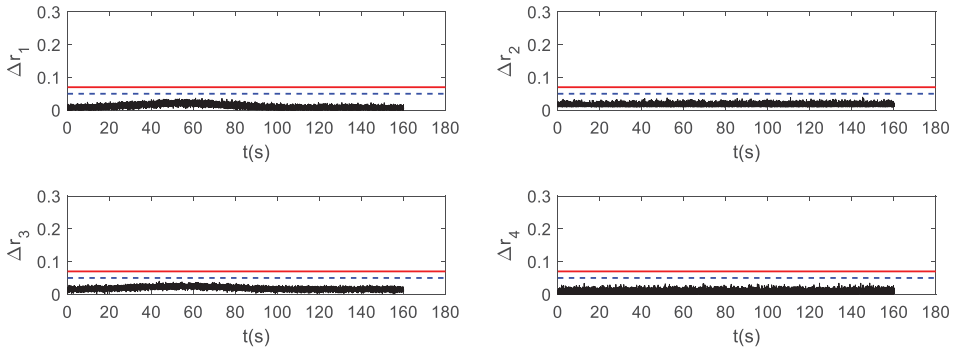


Figure 8. The ACEKF group diagram of the faultless state.

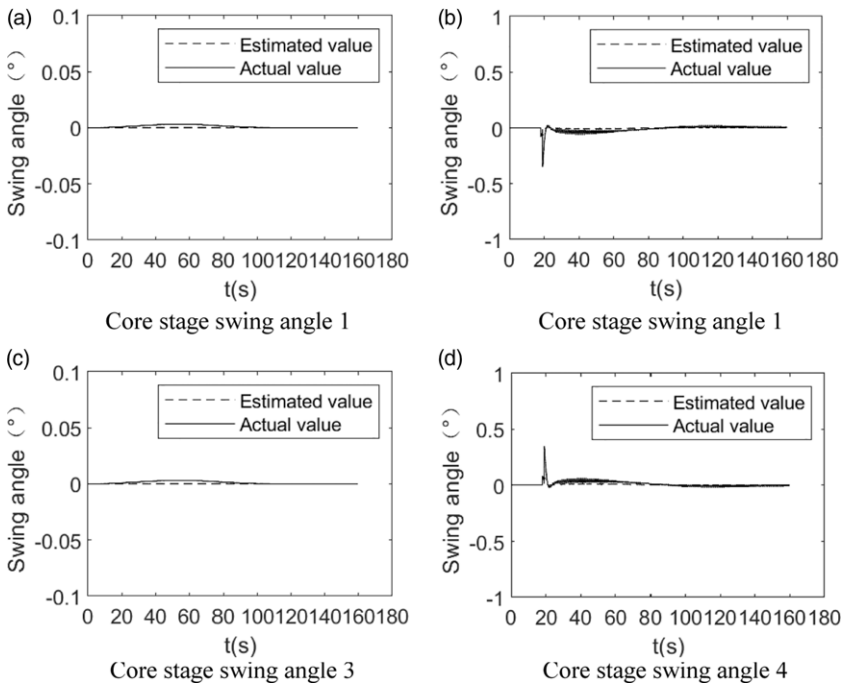


Figure 9. Simulation curve of core stage swing angle.

6.2 Sensor failure

Fault 1: A 0.5% constant bias fault occurred in the launch vehicle yaw angle measurement element at the 60s, i.e., a bias fault occurred in the corresponding sensor 1. Figure 8 shows the 1-SCKF residuals simulation curve after the bias fault occurs.

As demonstrated in Fig. 10, when sensor 1 fails, the related residuals surpass the threshold value, but the remainder of the Kalman filter residuals is unaffected, as shown in Fig. 7. As a result, sensor FDD is achieved.

6.3 Actuator failure

Fault 2: A jamming fault occurred in the launch vehicle actuator booster swing angle 1 (ABSA-1) at the 60s. Figure 11 depicts the SCKF bank residual simulation curve following the jamming fault, while Fig. 12 depicts the 5-ACEKF residual simulation curve.

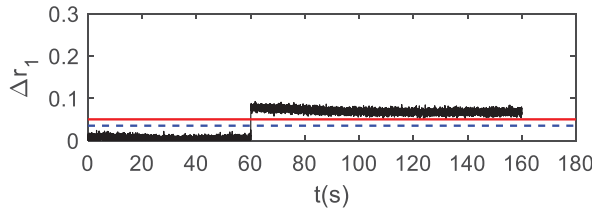


Figure 10. The 1-SCKF residual simulation curve at bias failure.

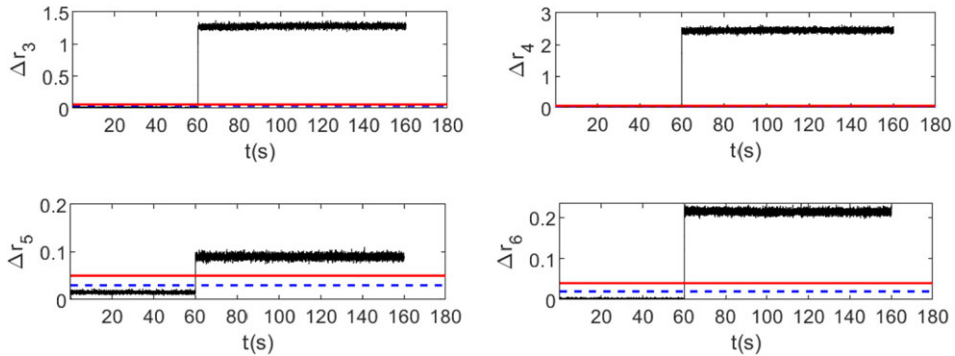


Figure 11. The SCKF group residual simulation curve at jamming fault.

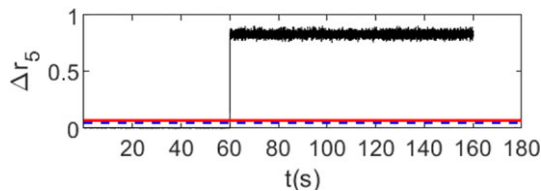


Figure 12. The 5-ACEKF residual simulation curve at jamming fault.

When the actuator fails, the residuals of the SCKF exceed threshold values in four sets, with Δr_4 (the WSSR of the pitch angle velocity) being the most sensitive to the failure of the ABSA-1, and the remainder of the residual curves still depicted in Fig. 7. According to the fault isolation method based on the MMFD algorithm described in Section 4.2, the actuator has failed at this moment.

From Fig. 12, it can be seen that the 5-ACEKF residual has changed abruptly and exceeded the set threshold value. So, the fault diagnosis result is that the ABSA-1 works normally until the jamming fault occurs at the 60s, thus, the FDD of the actuator can be achieved too.

According to the analysis in Sections 6.1–6.3, the construction of multiple Kalman filters can effectively isolate actuator and sensor faults in any mode, providing accurate information for subsequent FTC decisions.

6.4 Launch vehicle FTC

The preceding subsection implements the launch vehicle’s fault diagnosis using the MMFD algorithm, and the next step is to use the fault diagnostic information for FTC.

For sensor faults, the reconstructed sensor data are imported into the ACS for active FTC. Suppose a bias fault develops in sensor 1 with bias sizes of 0.5%, 0.8% and 1%, respectively. The following Figure 13 depicts the reconstructed results of the measured data following the occurrence of the bias fault.

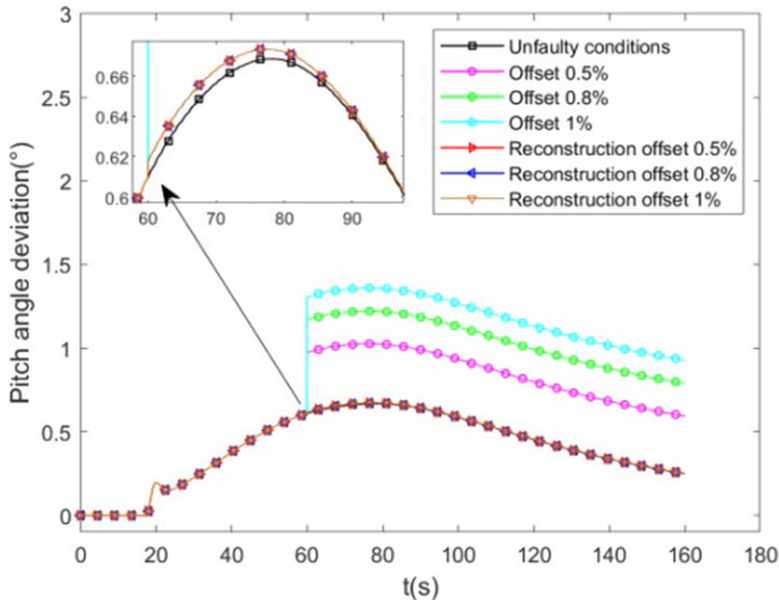


Figure 13. Attitude angle deviation curve under sensor bias fault.

Figure 13 shows the deviation curves of the pitch angle simulation results from the flight program angle, where the pitch angle simulation curve is corresponding to the measured data of sensor 1. When the sensor data is not reconstructed, the pitch angle deviation increases with increasing bias; after reconstruction, the pitch angle deviation decreases significantly. After a period of time when the failure occurs, the simulation curves after reconstruction with varied bias levels are consistent and near to the normal simulation curves because the measured values are replaced by the estimated values using the relevant Kalman filter. It can be seen that the reconstructed sensor data can meet the requirements of the launch vehicle ACS in terms of accuracy and stability.

For actuator faults, the fault information is brought into Equation (41), and the CDL is used to implement the redistribution of the swing angle for attitude FTC. In this paper, we conduct a control law reconstruction using all functioning core stages and booster engines.

Assume an ABSA-1 jamming failure occurs, with jamming angles of 4° , 6° and 8° , respectively. The following graph depicts the change in attitude angle once the stuck fault occurs.

Figure 14 shows that when a stuck fault occurs in the ABSA-1, the system can respond quickly, and the CAM starts to reconfigure. The fault mainly affects the yaw and roll channels, which appear a slight change at 60s, closely matching the residual variation characteristic in Fig. 11. The b: Stuck angle- 8° in Fig. 14(c) represents the roll angle curve of the stuck fault during the reconstruction without control law, when the curve does not converge at this time and the angular deviation is more than 12° . In contrast, the swing angle redistribution can effectively compensate for the torque loss and reduce the attitude angle deviation, whose roll angle error after reconfiguration does not exceed 0.05° (as shown in a: stuck angle- 8°).

Figure 15 shows the swing angle reconstruction curve of the actuator when the boost swing angle 1 is stuck at 8° . It can be seen from the figure that after the stuck fault occurs, both the remaining core stage and the boost swing angle will swing substantially, mainly because the system needs to provide more control moments to compensate for the lost control moment and the interference moment caused by the swing angle stuck. Because the core stage and boost swing angle do not exceed the maximum swing angle limit, the system still has a certain safety margin. It can also be seen from Fig. 15(e) that the ACEKF can accurately estimate the fault quantity, and the angle curve of boost swing angle 1 is consistent with the fault injection quantity.

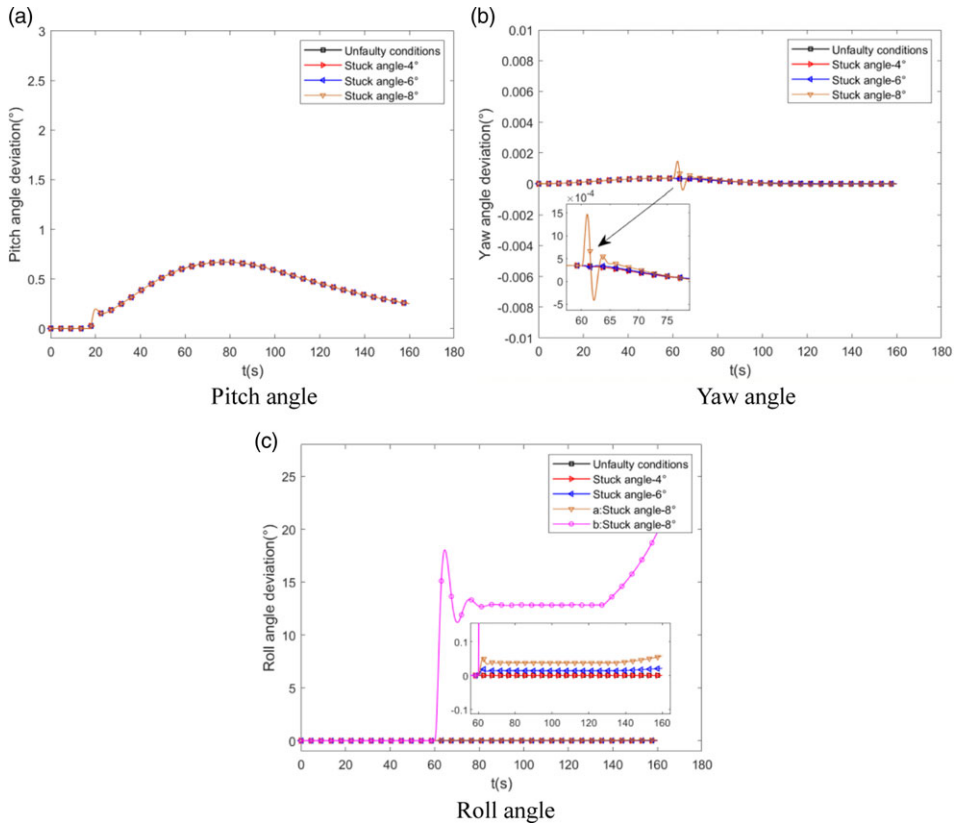


Figure 14. Attitude angle deviation curve under actuator jamming fault.

The following table lists the rocket roll Angle attitude control results under different control methods when the actuator is stuck. References (22,23), whose control object is still a large Chinese launch vehicle (Table 1).

In terms of control results, this method fully utilises the fault information to obtain the optimal control scheme, so the attitude tracking accuracy and control adjustment time are better than other methods. Although adaptive sliding film control can also achieve a better attitude control effect, it only models the actuator faults accordingly. In contrast, this paper considers arbitrary faults of the system sensors and actuators.

7.0 Conclusions

In this paper, the problem of fault diagnosis and fault-tolerant control of the launch vehicle attitude control system is investigated, and the effectiveness of the method is verified by fault simulation injection. The main contributions are as follows.

- (1) A launch vehicle ACS fault diagnosis algorithm is proposed. By analysing the fault characteristics of actuators and sensors, a Kalman filter with different structures is established, which realises the accurate identification of typical faults.
- (2) The FTC strategy for launch vehicle ACS is designed. Based on the above fault information, the actuator and sensor faults are automatically compensated by reconfiguring the attitude control

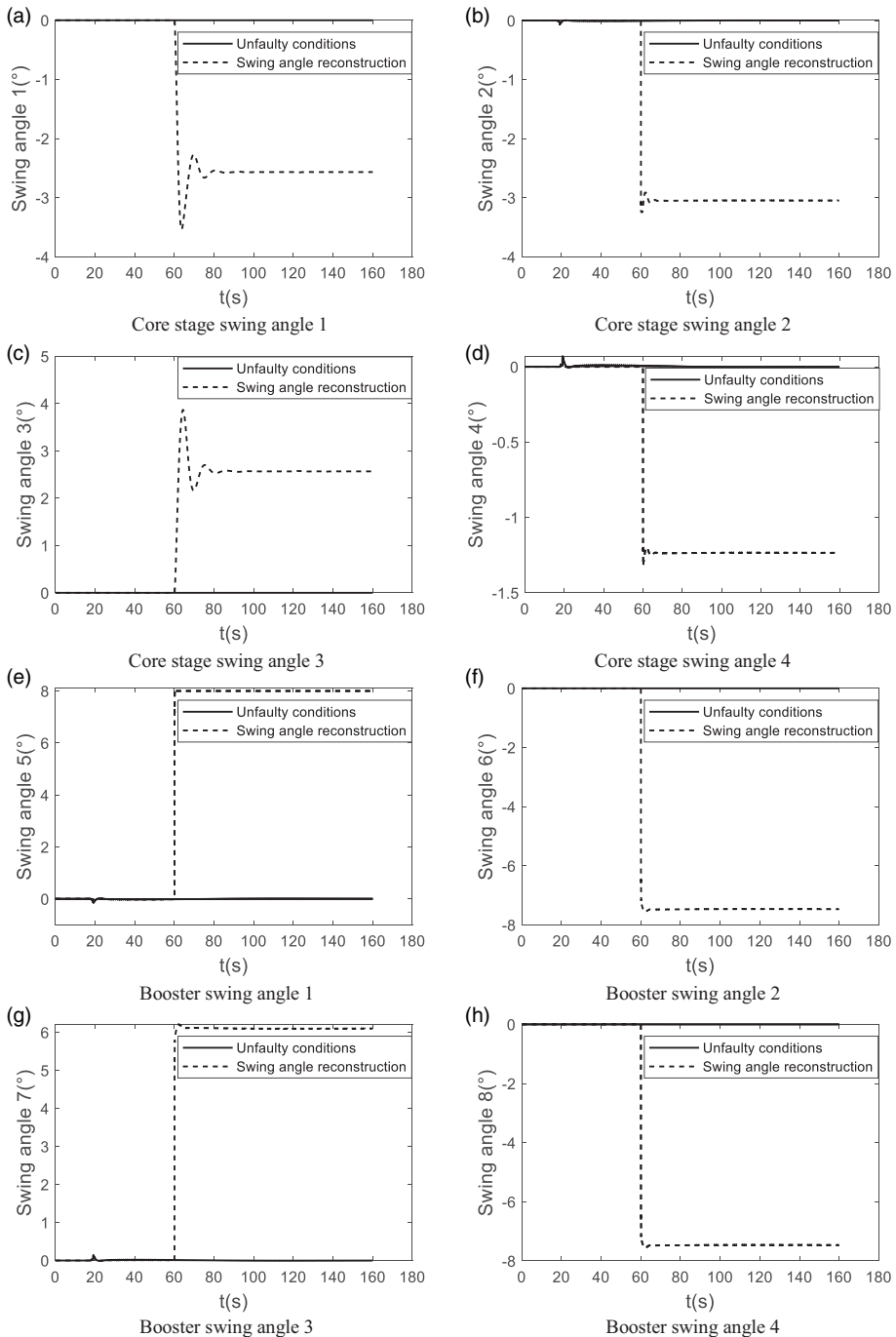


Figure 15. Simulation curve of swing angle after actuator fault reconstruction.

law. Compared with other control methods, the attitude tracking accuracy and control adjustment time are greatly improved, effectively ensuring the flight stability of the launch vehicle.

Further research may include the establishment of a semi-physical simulation environment to validate the active FTC method proposed in this paper, as well as the consideration of more typical fault models (e.g., valves, pipelines, etc.) to build observation models to improve the robustness of the ACS.

Table 1. Comparison of rocket roll angle attitude control results

Control method	Maximum deviation(°)	Steady-state deviation(°)	Control adjustment time(s)	Failure mode
PD control	18	18	50	Boost swing Angle stuck (8°)
Adaptive synovial control	0.042	0.042	13.5	Boost swing Angle stuck (3°)
Adaptive FTC control	7	2.5	10.2	Boost swing Angle stuck (8°)
Textual control method (MMFD + FTC)	0.043	0.032	7.3	Boost swing Angle stuck (8°)

Acknowledgments. The authors would like to thank the peer reviewers of the paper.

Competing interests. The authors declare that they have no known competing financial interests or personal relationships that could have appeared to influence the work reported in this paper.

References

- [1] Li D. and Li P. Technological breakthroughs of LM-5 and future developments of China's launch vehicle. *Acta Aeronaut. Astronaut. Sin.*, 2022, **43**, (10), p. 12. doi:10.7527/S1000-6893.2022.27269
- [2] Wang Z. Study on attitude control of heavy lift launch vehicle. (Doctoral dissertation, Huazhong university of science and technology, Wuhan), 2013. doi:10.7666/d.D411177
- [3] Rank P.M. Fault diagnosis in dynamic systems using analytical and knowledge based redundancy—a survey and some new results. *Automation*, 1990, **26**, (3), pp. 459–474. doi:10.1016/0005-1098(90)90018-D
- [4] Venkateswaran N., Siva M.S. and Goel P.S. (2002). Analytical redundancy based fault detection of gyroscopes in spacecraft applications. *Acta Astronautica*, **50**, (9), pp. 535–545. doi:10.1016/S0094-5765(01)00209-0
- [5] Caliskan F. and Hajiyev C. Active fault-tolerant control of UAV dynamics against sensor-actuator failures. *J. Aerosp. Eng.*, 2016, **29**, (4), p. 04016012. doi:10.1061/(ASCE)AS.1943-5525.0000579
- [6] Tang P., Lin D., Zheng D., Fan S. and Ye J. Observer based finite-time fault tolerant quadrotor attitude control with actuator faults. *Aerosp. Sci. Technol.*, 2020, **104**, p. 105968. doi:10.1016/j.ast.2020.105968
- [7] Bernardi E. and Adam E.J. Observer-based fault detection and diagnosis strategy for industrial processes. *J. Franklin Inst.*, 2020, **357**, (14). doi:10.1016/j.jfranklin.2020.07.046
- [8] Xiao B., Hu Q. and Wang D. Spacecraft attitude fault tolerant control with terminal sliding-mode observer. *J. Aerosp. Eng.*, 2015, **28**, (1), p. 04014055. doi:10.1061/(ASCE)AS.1943-5525.0000331
- [9] Hu C., Gao Z., Ren Y. and Liu Y. A robust adaptive nonlinear fault-tolerant controller via norm estimation for reusable launch vehicles. *Acta Astronaut.*, 2016, **128**, pp. 685–695. doi:10.1016/j.actaastro.2016.08.020
- [10] Lee T. and Youdan K. Nonlinear adaptive flight control using backstepping and neural networks controller. *J. Guid. Control Dyn.*, 2001. doi:10.2514/2.4794
- [11] Jing B., Zang K., Yang H., Cheng Y., Ma Y. and Cheng W. Fault tolerant control of satellite attitude control systems: review. *Acta Aeronaut. Astronaut. Sin.*, 2021, **42**, (11), p. 14. doi:10.7527/S1000-6893.2020.24662
- [12] Zhu S., Shen Q. and Danwei W. Finite-time fault-tolerant attitude stabilization for spacecraft with actuator saturation. *IEEE Trans. Aerosp. Electron. Syst.*, 2015.
- [13] Liang X., Hu C., Zhou Z. and Wang Q. ADP-based Intemgent attitude fault-tolerant control for launch vehicles. *Acta Aeronaut. Astronaut. Sin.*, 2021, **42**, (4), p. 14. doi:10.7527/S1000-6893.2020.24915
- [14] Gao Z., Zhou Z., Qian M.S., et al. Active fault tolerant control scheme for satellite attitude system subject to actuator time-varying faults[J]. *IET Control Theory Appl.*, 2018, **12**, (3), pp. 405–412.
- [15] Cao T., Gong H., Cheng P. and Xue Y. A novel learning observer-based fault-tolerant attitude control for rigid spacecraft. *Aerospace science and technology*, 2022, **128**, (9), pp. 107751.1–107751.14.
- [16] Perrett B. China launches new manned spacecraft with long March 5B. *Aerosp. Daily Defense Rep.*, 2020, **24**, p. 272.
- [17] Zhi W. On-line Trajectory Generation and Attitude Control System Reconstruction for Launch Vehicle with Thrust Decline. (MA thesis, School of National University of Defense Technology), 2016. doi:CNKI:CDMD:2.1018.997730
- [18] Yaakov Bar-Shalom X., Rong L. and Kirubarajan T. *State Estimation in Discrete-Time Linear Dynamic Systems*: John Wiley & Sons, Ltd., 2002.

[19] Li X., Xu F., Zhou W. and Ma H. *Redundant Inertial Group Reconstruction and Ballistic Replanning Technology of Launch Vehicle*: Science Press. (In Chinese), 2021.

[20] Theilliol D., Sauter D. and Ponsart J.C. A multiple model based approach for fault tolerant control in non-linear systems. *IFAC Proc. Vol.*, 2003, **36**, (5), pp. 149–154. doi:10.1016/S1474-6670(17)36485-6

[21] Wang J., Zhang D., Hong L. and Li N. Strategy on multi-rate gyroscopes application to attitude control of launch vehicles. *J. Astronaut.*, 2020, **41**, (3), p. 337. doi:10.3873/j.issn.1000-1328.2020.03.010

[22] Ma Y., Shi X., Liu H., Liang X. and Wang Q. Adaptive neural network fault tolerant control of launch vehicle attitude system. *J. Astronaut.*, 2021, **42**, (10), p. 9. doi:10.3873/j.issn.1000-1328.2021.10.005

[23] Meng Z. Fault tolerant control for large strap-on Launch vehicle's servomechanism. (Doctoral dissertation, School of National University of Defense Technology), 2013. doi:10.7666/d.D675848

[24] Yang S., Xie C., Cheng Y., Song D. and Cui M. Autonomous attitude reconstruction analysis for propulsion system with typical thrust drop fault. *Aerospace*, 2022, **9**, p. 409. doi:10.3390/aerospace9080409

Appendix A

In Ref. (24), a small deviation attitude dynamics model of the launch vehicle has been derived. For rocket reconstruction design, considering that the engine swing is very small in the whole flight process, and the motion of the arrow body is a short period process, the effects of the pendulum angle acceleration term caused by the engine swing and the rocket centre of mass motion can be ignored. For the following equation:

$$\Delta\varphi = \Delta\theta + \Delta\alpha$$

$$\psi = \sigma + \beta$$

After simplification can be obtained,

$$\Delta\varphi = \Delta\alpha$$

$$\Delta\psi = \Delta\beta$$

Then the simplified small-deviation dynamic equation of rocket around the centre of mass is,

$$\begin{aligned} \Delta\ddot{\varphi} + b_1^\varphi \Delta\dot{\varphi} + b_2^\varphi \Delta\varphi - b_{3xj2}^\varphi \Delta\delta_{xj2} + b_{3xj1}^\varphi \Delta\delta_{xj4} - b_{3zr2}^\varphi \Delta\delta_{zr2} + b_{3zr4}^\varphi \Delta\delta_{zr4} \\ = \bar{M}_{BZ_1} - b_2^\varphi (\alpha_{wp} + \alpha_{wq}) \\ \ddot{\psi} + b_1^\psi \dot{\psi} + b_2^\psi \psi - b_{3xj1}^\psi \Delta\delta_{xj1} + b_{3xj2}^\psi \Delta\delta_{xj3} - b_{3zr1}^\psi \Delta\delta_{zr1} + b_{3zr3}^\psi \Delta\delta_{zr3} \\ = \bar{M}_{BY_1} - b_2^\psi (\beta_{wp} + \beta_{wq}) \\ \ddot{\gamma} + d_1 \dot{\gamma} + d_{3xj1} \delta_{xj1} + d_{3xj2} \delta_{xj2} + d_{3xj3} \delta_{xj3} + d_{3xj4} \delta_{xj4} + d_{3zr1} \delta_{zr1} + d_{3zr2} \delta_{zr2} \\ + d_{3zr3} \delta_{zr3} + d_{3zr4} \delta_{zr4} = \bar{M}_{BX_1} \end{aligned}$$

where,

$$\left\{ \begin{aligned} b_1^\varphi &= \frac{qS_M m_{dc} l^2}{J_{Z_1} V}, b_2^\varphi = \frac{qS_M C_n^\alpha (x_d - x_T)}{J_{Z_1}} \\ b_{3xj1}^\varphi &= \frac{k_{xj1} P_{xj} (x_{Rxj} - x_T) + m_{Rxj} \dot{W}_{X_1} l_{Rxj}}{J_{Z_1}}, b_{3xj2}^\varphi = \frac{k_{xj2} P_{xj} (x_{Rxj} - x_T) + m_{Rxj} \dot{W}_{X_1} l_{Rxj}}{J_{Z_1}} \\ b_{3zr2}^\varphi &= \frac{k_{zr2} P_{zr} (x_{Rzr} - x_T) + m_{Rzr} \dot{W}_{X_1} l_{Rzr}}{J_{Z_1}}, b_{3zr4}^\varphi = \frac{k_{zr4} P_{zr} (x_{Rzr} - x_T) + m_{Rzr} \dot{W}_{X_1} l_{Rzr}}{J_{Z_1}} \\ \bar{M}_{BZ_1} &= \frac{M_{BZ_1}}{J_{Z_1}} \end{aligned} \right.$$

$$\begin{cases} b_1^\psi = \frac{qS_M m_{dy} l^2}{J_{Y_1} V}, b_2^\psi = \frac{qS_M C_n^\beta (x_d - x_T)}{J_{Y_1}} \\ b_{3xj1}^\psi = \frac{k_{xj1} P_{xj} (x_{Rxj} - x_T) + m_{Rxj} \dot{W}_{X_1} l_{Rxj}}{J_{Y_1}}, b_{3xj2}^\psi = \frac{k_{xj2} P_{xj} (x_{Rxj} - x_T) + m_{Rxj} \dot{W}_{X_1} l_{Rxj}}{J_{Y_1}} \\ b_{3z1}^\psi = \frac{k_{z1} P_{zt} (x_{Rzt} - x_T) + m_{Rzt} \dot{W}_{X_1} l_{Rzt}}{J_{Y_1}}, b_{3z3}^\psi = \frac{k_{z3} P_{zt} (x_{Rzt} - x_T) + m_{Rzt} \dot{W}_{X_1} l_{Rzt}}{J_{Y_1}} \\ \bar{M}_{BY_1} = \frac{M_{BY_1}}{J_{Y_1}} \\ d_1 = \frac{qS_M m_{dy} l^2}{J_{X_1} V} \\ d_{3xj1} = \frac{\sqrt{2} k_{xj1} P_{xj} r_0}{2J_{X_1}}, d_{3xj2} = \frac{\sqrt{2} k_{xj2} P_{xj} r_0}{2J_{X_1}}, d_{3xj3} = \frac{\sqrt{2} k_{xj3} P_{xj} r_0}{2J_{X_1}}, d_{3xj4} = \frac{\sqrt{2} k_{xj4} P_{xj} r_0}{2J_{X_1}} \\ d_{3z1} = \frac{k_{z1} P_{zt} r_1}{J_{X_1}}, d_{3z2} = \frac{k_{z2} P_{zt} r_1}{J_{X_1}}, d_{3z3} = \frac{k_{z3} P_{zt} r_1}{J_{X_1}}, d_{3z4} = \frac{k_{z4} P_{zt} r_1}{J_{X_1}} \\ \bar{M}_{BX_1} = \frac{M_{BX_1}}{J_{X_1}} \end{cases}$$

After the three-channel control instructions $\delta_\varphi^s, \delta_\psi^s, \delta_\gamma^s$ are calculated according to the basic control law, they are allocated to the core stage three channels and boost three channels according to the pre-designed distribution ratio, that is,

$$\begin{cases} \Delta \delta_{\varphi xj}^s = k_{xj} \Delta \delta_\varphi^s \\ \delta_{\psi xj}^s = k_{xj} \delta_\psi^s \\ \delta_{\gamma xj}^s = k_{xj} \delta_\gamma^s \end{cases}, \begin{cases} \Delta \delta_{\varphi zt}^s = k_{zt} \Delta \delta_\varphi^s \\ \delta_{\psi zt}^s = k_{zt} \delta_\psi^s \\ \delta_{\gamma zt}^s = k_{zt} \delta_\gamma^s \end{cases}$$

The actuator distributes the obtained instructions to each engine according to the pre-designed control distribution law, which can be obtained,

$$\begin{cases} \delta_{xj1} = -\delta_{\psi xj}^s + \delta_{\gamma xj}^s \\ \delta_{xj2} = -\Delta \delta_{\varphi xj}^s + \delta_{\gamma xj}^s \\ \delta_{xj3} = \delta_{\psi xj}^s + \delta_{\gamma xj}^s \\ \delta_{xj4} = \Delta \delta_{\varphi xj}^s + \delta_{\gamma xj}^s \end{cases}, \begin{cases} \delta_{zt1} = -\delta_{\psi zt}^s + \delta_{\gamma zt}^s \\ \delta_{zt2} = -\Delta \delta_{\varphi zt}^s + \delta_{\gamma zt}^s \\ \delta_{zt3} = \delta_{\psi zt}^s + \delta_{\gamma zt}^s \\ \delta_{zt4} = \Delta \delta_{\varphi zt}^s + \delta_{\gamma zt}^s \end{cases}$$

The above is the basic control law of the arrow body when there is no thrust fault. When a fault occurs, the original control distribution law is no longer applicable, and the engine swing angle needs to be redistributed so that the control torque obtained after reallocation is equal to the expected control torque, and formula (40) is obtained, the relevant symbolic meanings of the derivation process are shown in Table 2.

$$\begin{bmatrix} b_{3x}^\varphi \Delta \delta_{\varphi xj}^s + b_{3z}^\varphi \Delta \delta_{\varphi zt}^s \\ b_{3x}^\psi \delta_{\psi xj}^s + b_{3z}^\psi \delta_{\psi zt}^s \\ d_{3x} \delta_{\gamma xj}^s + d_{3z} \delta_{\gamma zt}^s \end{bmatrix} = \begin{bmatrix} 0 & -b_{3xj2}^\varphi & 0 & b_{3xj1}^\varphi & 0 & -b_{3z2}^\varphi & 0 & b_{3z4}^\varphi \\ -b_{3xj1}^\psi & 0 & b_{3xj2}^\psi & 0 & -b_{3z1}^\psi & 0 & b_{3z3}^\psi & 0 \\ d_{3x1} & d_{3x2} & d_{3x3} & d_{3x4} & d_{3z1} & d_{3z2} & d_{3z3} & d_{3z4} \end{bmatrix} \times \begin{bmatrix} \delta_x \\ \delta_z \end{bmatrix}$$

Table 2. The basic symbol meaning

Symbol	The symbolic meaning
S_m	Maximum cross-sectional area of the rocket
l	The rocket length
$J_{X_1}, J_{Y_1}, J_{Z_1}$	The moment of inertia of the rocket in the coordinate system around the arrow body ($O_1 - X_1 Y_1 Z_1$)
$m_{R_{xj}}, m_{R_{zt}}$	The core stage/boost engine mass
$l_{R_{xj}}, l_{R_{zt}}$	The distance from the centre of mass of the core stage/booster engine to the corresponding hinge shaft
r_0, r_1	The distance from the core stage/booster engine thrust operation point to the rocket axis of symmetry
$x_{R_{xj}}, x_{R_{zt}}$	The distance from the engine hinge shaft to the top of the rocket
x_T	The distance between the rocket's centre of mass and the rocket's tip from the rocket's axis of symmetry
x_d	The distance from the rocket's pneumatic centre to the top of the rocket
xj_1, xj_2	The two core engines
$z1_1, z1_2, z1_3, z1_4$	The four booster engines
$\delta_{xj1}, \delta_{xj2}, \delta_{xj3}, \delta_{xj4}$	Core stage swing angle
$\ddot{\delta}_{xj1}, \ddot{\delta}_{xj2}, \ddot{\delta}_{xj3}, \ddot{\delta}_{xj4}$	Core stage swing angle acceleration
$\delta_{zt1}, \delta_{zt2}, \delta_{zt3}, \delta_{zt4}$	Boost swing angle
$\ddot{\delta}_{zt1}, \ddot{\delta}_{zt2}, \ddot{\delta}_{zt3}, \ddot{\delta}_{zt4}$	Boost swing angle acceleration
$\Delta\delta_{\varphi_{xj}}, \Delta\delta_{\psi_{xj}}, \Delta\delta_{\gamma_{xj}}$	Core level three channel swing angle command
$\Delta\delta_{\varphi_{zt}}, \Delta\delta_{\psi_{zt}}, \Delta\delta_{\gamma_{zt}}$	Boost three channel swing angle command
$\Delta\delta_{\varphi}, \Delta\delta_{\psi}, \Delta\delta_{\gamma}$	Virtual swing angle instruction
P_{xj}, P_{zt}	Core stage/booster engine thrust
$k_{xj1}, k_{xj2}, k_{zt1}, k_{zt2}, k_{zt3}, k_{zt4}$	Proportional coefficient of thrust reduction of each engine
$M_{BZ1}, M_{BY1}, M_{BX1}$	Structural disturbance torque around the arrow body coordinate system direction
V	Flight centre of mass velocity
\dot{W}	Apparent acceleration
φ, ψ, γ	Pitch/ yaw/ roll angle
θ	Velocity dip
σ	Track drift angle
ν	Angle of heel
β	Sideslip angle
α	Angle-of-attack
α_{wp}, α_{wq}	Additional angle of attack caused by smooth and shear winds
β_{wp}, β_{wq}	Additional sideslip angle caused by smooth wind and shear wind
C_n^α, C_n^β	The derivative of rocket normal force coefficient with respect to angle of attack and sideslip angle
m_{dx}, m_{dy}, m_{dz}	The torque coefficient corresponding to the aerodynamic torque
$q = \frac{1}{2} \rho (\square) \tilde{V}^2$	q : Kinetic pressure $\rho(h)$: Atmospheric density at altitude h \tilde{V} : The velocity of the rocket relative to the atmosphere during flight can be approximated as $\tilde{V} = V$

Cite this article: Chang-lin X., Shu-ming Y., Yu-qiang C. and Li-jun S. (2024). Multiple model fault diagnosis and fault tolerant control for the launch vehicle's attitude control system. *The Aeronautical Journal*, **128**, 1875–1894. <https://doi.org/10.1017/aer.2024.14>